

The 750 GeV Diphoton Excess May Not Imply a 750 GeV Resonance

Won Sang Cho,¹ Doojin Kim,² Kyoungchul Kong,³ Sung Hak Lim,^{1,4}
Konstantin T. Matchev,² Jong-Chul Park,⁵ and Myeonghun Park¹

¹*Center for Theoretical Physics of the Universe,
Institute for Basic Science (IBS), Daejeon, 34051, Korea*

²*Department of Physics, University of Florida, Gainesville, FL 32611, USA*

³*Department of Physics and Astronomy, University of Kansas, Lawrence, KS 66045, USA*

⁴*Department of Physics, KAIST, 291 Daehak-ro, Yuseong-gu, Daejeon, 34141, Korea*

⁵*Department of Physics, Chungnam National University, Daejeon 305-764, Korea*

(Dated: June 7, 2022)

We discuss non-standard interpretations of the 750 GeV diphoton excess recently reported by the ATLAS and CMS Collaborations which do *not* involve a new, relatively broad, resonance with a mass near 750 GeV. Instead, we consider the sequential cascade decay of a much heavier, possibly quite narrow, resonance into two photons along with one or more invisible particles. The resulting diphoton invariant mass signal is generically rather broad, as suggested by the data. We examine three specific event topologies — the “antler”, the “sandwich”, and the 2-step cascade decay, and show that they all can provide a good fit to the observed published data. In each case, we delineate the preferred mass parameter space selected by the best fit. In spite of the presence of invisible particles in the final state, the measured missing transverse energy is moderate, due to its anti-correlation with the diphoton invariant mass. We comment on the future prospects of discriminating with higher statistics between our scenarios, as well as from more conventional interpretations.

PACS numbers: 14.80.-j,12.60.-i

Introduction. Recently, the ATLAS and CMS Collaborations have reported first results with data obtained at the Large Hadron Collider (LHC) operating at 13 TeV. The data shows an intriguing excess in the inclusive diphoton final state [1, 2]. The ATLAS Collaboration further reported that about 15 events in the diphoton invariant mass distribution are observed above the Standard Model (SM) expectation at 3.9σ local significance (2.3σ global significance) with 3.2 fb^{-1} of data. The excess appears as a bump at $M \sim 750 \text{ GeV}$ with a relatively broad width $\Gamma \sim 45 \text{ GeV}$, resulting in $\Gamma/M \sim 0.06$ [1]. Similar results are reported by the CMS Collaboration for 2.6 fb^{-1} of data — there are about 10 excess events at a local significance of 2.6σ (2.0σ) assuming a narrow (wide) width [2]. The anomalous events are not accompanied by significant missing energy, or jet or lepton multiplicity. The required cross section for the excess is $\sim 10 \text{ fb}$ at 13 TeV, and so far no indication of a similar excess has been observed in other channels.

While waiting for the definitive verdict on this anomaly from additional LHC data, it is fun to speculate on new physics scenarios which are consistent with the current data. Since the excess was seen in the diphoton invariant mass spectrum, the most straightforward interpretation would involve the production of a resonance with mass near 750 GeV, which decays directly to two photons. The relative broadness of the observed feature in turn would imply that this resonance has a relatively large width, creating some tension with its non-observation in other channels. Since the initial announcement, many models along those lines have been proposed [3].

In this letter, we entertain a different interpretation of the diphoton excess in the context of a sequential cas-

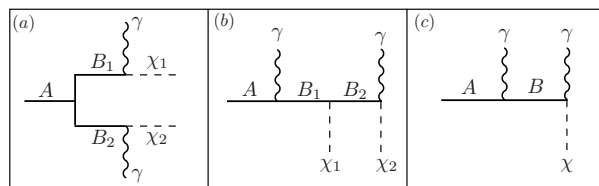


FIG. 1: The event topologies with two photons and up to two invisible particles under consideration in this letter: (a) antler, (b) sandwich, and (c) 2-step cascade decay. Wavy lines denote photons, dotted lines represent invisible, weakly interacting, particles (χ_i) which could be dark matter candidates, while solid lines correspond to heavier resonances (A, B_i).

cade decay of a much heavier, possibly quite narrow, resonance, resulting in a final state with two photons and one or two *invisible* particles. Three specific examples of such simplified model event topologies are exhibited in Fig. 1: an “antler” topology [4] in Fig. 1(a), a “sandwich” topology [5] in Fig. 1(b) and a 2-step cascade decay in Fig. 1(c). In such scenarios, the resulting diphoton invariant mass is typically characterized by a somewhat broad distribution, which eliminates the necessity of an intrinsically broad resonance. Furthermore, the peak of the diphoton mass distribution is found near the upper kinematic endpoint, making it likely that the first signal events will be seen at large invariant mass, while the low mass tail remains buried under the steeply falling SM background. Interestingly, for signal events with the required extreme values of the diphoton mass, the missing transverse momentum turns out to be rather moderate, due to its anti-correlation with the diphoton mass. Given

the small signal statistics ($\mathcal{O}(10)$ events) such cascade decays may easily fake the standard diphoton resonance signature, and deserve further scrutiny.

Diphoton invariant mass spectrum. We first review the diphoton invariant mass distributions corresponding to the above-mentioned three event topologies from Fig. 1. The differential distribution of the diphoton invariant mass $m \equiv m_{\gamma\gamma}$

$$\frac{dN}{dm} \equiv f(m; M_A, M_{B_i}, M_{\chi_i}) \quad (1)$$

is known analytically (see, e.g., [6]) and is simply a function of the unknown masses M_A , M_{B_i} and M_{χ_i} . The kinematic endpoint (henceforth denoted as E) is defined as the maximum value of m allowing a non-zero $f(m)$, i.e., $E \equiv \max\{m\}$.

Ignoring for the moment spin correlations and assuming pure phase space distributions, the shape in the case of the antler topology of Fig. 1(a) is given by [4]

$$f(m) \sim \begin{cases} \eta m, & 0 \leq m \leq e^{-\eta} E, \\ m \ln(E/m), & e^{-\eta} E \leq m \leq E, \end{cases} \quad (2)$$

where the endpoint E and the parameter η are defined in terms of the mass parameters as

$$E = \sqrt{e^\eta (M_{B_1}^2 - M_{\chi_1}^2)(M_{B_2}^2 - M_{\chi_2}^2) / (M_{B_1} M_{B_2})}, \quad (3)$$

$$\eta = \cosh^{-1} [(M_A^2 - M_{B_1}^2 - M_{B_2}^2) / (2M_{B_1} M_{B_2})]. \quad (4)$$

The corresponding shape for the sandwich topology is given by the same expression (2), only this time E and η are defined as follows [6]:

$$E = \sqrt{e^\eta (M_A^2 - M_{B_1}^2)(M_{B_2}^2 - M_{\chi_2}^2) / (M_{B_1} M_{B_2})}, \quad (5)$$

$$\eta = \cosh^{-1} [(M_{B_1}^2 + M_{B_2}^2 - M_{\chi_1}^2) / (2M_{B_1} M_{B_2})]. \quad (6)$$

Finally, the two-step cascade decay has the well-known triangular shape

$$f(m) \sim m, \quad (7)$$

where the distribution extends up to

$$E = \sqrt{(M_A^2 - M_B^2)(M_B^2 - M_\chi^2) / M_B^2}. \quad (8)$$

Fig. 2 displays unit-normalized distributions for the theoretical results (2) and (7) (black dashed lines) overlaid with Monte Carlo simulation results (solid line histograms) obtained with the phase space generator in ROOT [7], for all three event topologies. The left panel of Fig. 2 shows the two identical cases of Fig. 1(a) and Fig. 1(b). Here we take five representative η values to demonstrate the dependence of the peak position on η — for small enough values of η , the peak can be arbitrarily close to the endpoint. The right panel in Fig. 2 corresponds to Fig. 1(c). In all cases (assuming small enough values of η in (2)), the distributions are characterized by a relatively broad peak near the kinematic

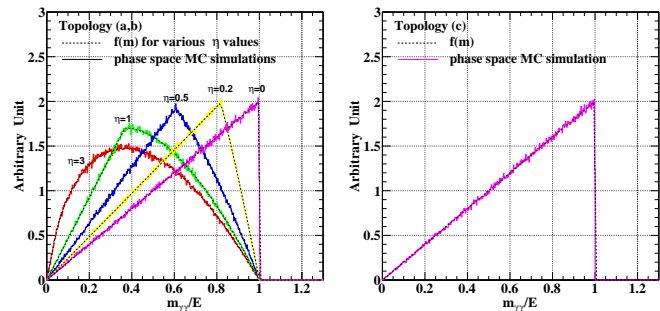


FIG. 2: Unit-normalized theory expectations (black dashed curves) of $f(m)$ and the corresponding Monte Carlo simulation (colored histogram) for the event topologies of Fig. 1(a,b) (left panel) and Fig. 1(c) (right panel).

endpoint, and a continuously falling tail to lower values of m . Given that the SM background distribution for $m_{\gamma\gamma}$ is a very steeply falling function, the low m tail can be easily hidden in the background, and the only feature of the distributions in Fig. 2 which would be visible in the early data is the peak itself.

Data analysis. Given the analytical results (2-8) from the previous section, we now try to fit the three models from Fig. 1 to the $m_{\gamma\gamma}$ spectrum data reported by the ATLAS Collaboration [1] (black dots in Fig. 3). To describe the background portion in the data, we introduce the same background model function as in [1]:

$$f_{bg}(x; b, a) = (1 - x^{1/3})^b x^a, \quad (9)$$

where a and b are fit parameters to be determined by data and $x = m/\sqrt{s}$ with $\sqrt{s} = 13$ TeV. We then perform likelihood fits using combined signal + background templates using $f(m)$ from Eqs. (2, 7) and $f_{bg}(m)$ from Eq. (9). Our fit results for the case of Fig. 1(a-b) (Fig. 1(c)) are shown in the upper (lower) panel of Fig. 3. The red solid curves represent the best-fit models (i.e., signal+background), while the red dashed (blue solid) curves describe their background (signal) components. To estimate parameter errors more carefully with low statistics, we generate 10,000 pseudo data sets via random samplings of the data point in each bin, assuming a Poisson distribution with the mean value set to its original one. We then conduct the same fit procedure explained above for all pseudo data sets and obtain distributions of fitted model parameters, from which we extract mean values and 1σ confidence intervals for them, along with reduced χ^2 distributions.

For the antler and sandwich cases, the relevant reduced χ^2 distribution yields a mean (median) value of 0.98 (0.93) with the Gaussian width around 1, indicating that our fitting template accommodates pseudo data samples well enough. The extracted best-fit parameter values and their 1σ errors are

$$\eta = 0.0322_{-0.0317}^{+0.0296}, \quad E = 827.0_{-36.9}^{+30.3} \text{ GeV}. \quad (10)$$

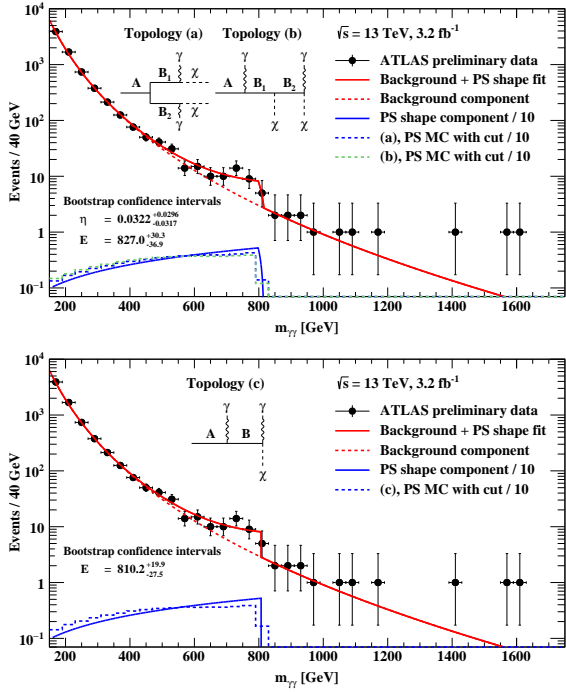


FIG. 3: Upper panel: the ATLAS diphoton data (black dots) and our fit results with the antler and sandwich event topologies, Eq. (2). The red solid curve represents the best-fit assuming pure phase space signal plus background distribution modelled by Eq. (9). The blue dashed (green dashed) curve represents the best-fit Monte Carlo event distribution in the antler (sandwich) case after incorporating the ATLAS analysis cuts. Lower panel: the same, but for the 2-step cascade decay of Fig. 1(c).

Due to the set of cuts applied in the ATLAS analysis to suppress the SM backgrounds, the resulting signal distributions could be distorted. In order to account for those effects, we (here and henceforth) take gg -induced single production of scalar A of $M_A = 1.7$ TeV with the LHC13, and let it decay according to a mass spectrum accommodating the best-fit E and η from Eq. (10). We then impose the selection cuts as in Ref. [1], and numerically reconstruct the signal template using the surviving events. Since the antler and the sandwich scenarios have, in principle, different cut-sensitivity, we show the corresponding distributions with the blue (antler) and green (sandwich) dashed curves in the upper panel of Fig. 3.

For the two-step cascade scenario, the relevant reduced χ^2 distribution shows a mean (median) value of 0.69 (0.67) with the Gaussian width around 0.5, indicating that this model also reproduces the data well enough. The best-fit value for E and its 1σ error are reported as

$$E = 810.2^{+19.9}_{-27.5} \text{ GeV}. \quad (11)$$

As before, the signal distribution after cuts is shown by the blue dashed curve in the lower panel of Fig. 3.

Discussions and outlook. Since the number of experimentally measurable parameters for the antler topol-

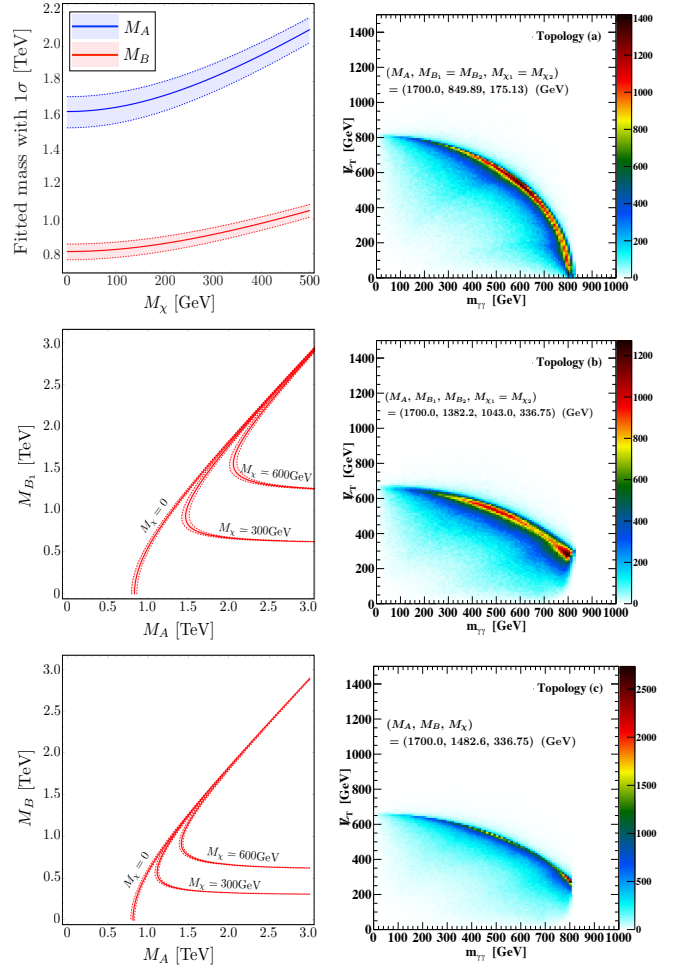


FIG. 4: Left panels: the allowed mass regions at 1σ , selected by the best-fit. Right panels: temperature plots showing the correlation between $m_{\gamma\gamma}$ and \cancel{E}_T , using Monte Carlo events with a representative mass spectrum consistent with the best-fit values in Eqs. (10) and (11).

ogy is two (namely, η and E) [6], the underlying mass spectrum is not fully determined. However, a phenomenologically motivated scenario is the case where the decay is symmetric, i.e., $B_1 = B_2$ and $\chi_1 = \chi_2$. We then have three input mass parameters, two of which can be given as functions of the third mass, using the measured values for η and E . Taking M_χ as a free parameter, we find that M_A and M_B can be expressed as follows:

$$M_B = \left(e^{-\eta/2} E + \sqrt{e^{-\eta} E^2 + 4M_\chi^2} \right) / 2, \quad (12)$$

$$M_A = \sqrt{2M_B^2 (\cosh \eta + 1)}. \quad (13)$$

The upper-left panel of Fig. 4 displays the corresponding 1σ mass ranges for the A (blue region and curves) and B (red region and curves) particles as a function of M_χ .

For the sandwich topology of Fig. 1(b), we can similarly reduce the number of input mass degrees of freedom by considering the simple case of $\chi_1 = \chi_2$ as a well-

motivated phenomenological scenario. Then, using the measurements (10), we can predict the masses of two of the unknown particles, say M_{B_1} and M_{B_2} , as a function of the other two, M_A and M_χ , as shown in the middle left panel of Fig. 4 (M_{B_1} only for illustration).

Finally, for the two-step cascade topology of Fig. 1(c), only one parameter, Eq. (11), can be measured from the data. This provides one relation among the three unknown masses M_A , M_B and M_χ , which is depicted in the bottom left panel of Fig. 4.

As mentioned earlier, the interesting events contributing to the excess do not seem to be accompanied by substantial missing transverse momentum. On the other hand, the three scenarios considered here have invisible particles in the final state, and one might naively expect that they would be in contradiction with the data. However, note that the events contributing to the excess are typically populated near the kinematic endpoint (see Figs. 2 and 3). For such events, the typical angular separation (in the laboratory frame) between the two photons is anticipated to be large. Now consider the antler event topology of Fig. 1(a), where each particle B decays into a photon and a χ . If the photons are almost back-to-back, then so must be the two χ 's, yielding a relatively small net missing transverse momentum. This inverse correlation between $m_{\gamma\gamma}$ and \cancel{E}_T is shown in the right panels of Fig. 4, where for completeness we also provide similar temperature plots for the sandwich and the two-step cascade decay topologies. In the left panel of Fig. 5, we show \cancel{E}_T distributions of simulated events around $m_{\gamma\gamma} \sim 700 - 800$ GeV (near the measured peak position) with the same mass spectra as in the right panels of Fig. 4. Again, the selection cuts adopted in Ref. [1] have been imposed. We clearly see that the antler scenario favors small \cancel{E}_T as expected. Certainly, once more data is accumulated, the missing transverse momentum will eventually be a good discriminator between the conventional resonance scenario (in which no \cancel{E}_T is expected) and a cascade decay scenario involving invisible particles.

An alternative handle to discriminate among these competing interpretations is provided by the photon energy spectrum. In the conventional case of a single resonance scenario with a large decay width [3], the photon energy spectrum has a unique peak at half the resonance mass [8, 9], and the peak may show a sharp kink structure if the heavy resonance is singly produced [10]. On the other hand, the energy distribution for the (symmetric) antler scenario develops a peak at

$$E_\gamma = (M_B^2 - M_\chi^2)/(2M_B), \quad (14)$$

which is, in principle, different from the peak in the $m_{\gamma\gamma}$ distribution. For the other two cases, the corresponding photon spectrum could develop a *double-bump* structure depending on the underlying mass spectrum [11]. These expectations are summarized in the right panel of Fig. 5.

Finally, we note the potential impact of spin correlations on our analysis. It is well-known that the overall shape of invariant mass distributions can be distorted by

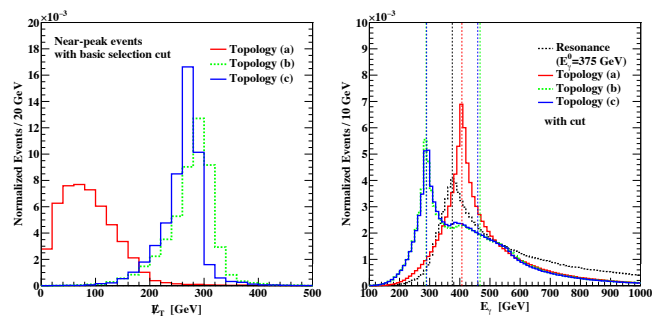


FIG. 5: Left panel: \cancel{E}_T distributions of events near the peak position. The mass spectra are the same as in the right panels of Fig. 4. Right panel: Photon energy distributions for the conventional scenario with a heavy resonance of mass 750 GeV and width 45 GeV (black dotted line), and the three cascade decay scenarios: the antler topology (red solid), the sandwich topology (blue solid), and the two-step cascade (green dotted). The dashed vertical lines mark the expected energy-peak locations.

the introduction of non-trivial spin correlations [12, 13]. One could then repopulate most of the signal events in a (relatively) narrow region around the peak, which would further improve the fit. Let $f_S(m)$ be the relevant $m_{\gamma\gamma}$ distribution in the presence of spin correlations. For the antler and sandwich cases, one can write [5, 14]

$$f_S(m) \sim \begin{cases} m(c_1 + c_2 t + c_3 t^2), & 0 \leq m \leq e^{-\eta} E, \\ m[c_4 + c_5 t + c_6 t^2 \\ + (c_7 + c_8 t + c_9 t^2) \ln t], & e^{-\eta} E \leq m \leq E. \end{cases} \quad (15)$$

Here $t \equiv m^2/E^2$ and c_i ($i = 1, \dots, 9$) represent coefficients encoding the underlying spin information. For the decay topology in Fig. 1(c), the relevant expression is given by the first line of Eq. (15) [5, 12]:

$$f_S(m) \sim m(d_1 + d_2 t + d_3 t^2) \text{ for } 0 \leq m \leq E, \quad (16)$$

and the presence of the additional terms beyond Eq. (7) can also favorably sculpt the distribution in the vicinity of the peak.

In conclusion, we investigated the nature of the anomalous excesses reported by the ATLAS and CMS Collaborations in terms of cascade decay topologies from a heavy, possibly quite narrow, resonance. Our scenarios can generically accommodate a (relatively) large width of the peak accompanied with a (relatively) small missing transverse momentum. The presence of invisible particles in the final state opens the door for discovery of not just a new particle beyond the Standard Model, but possibly of the dark matter. We also discussed the potential of distinguishing the competing interpretations with more data, using the missing transverse momentum and photon energy distributions. We eagerly await the resolution of this puzzle with new data from the LHC.

Acknowledgments

DK, KK and JCP thank CTPU-IBS for hospitality and support during the completion of this work. DK and KM thank the organizers of the Miami 2015 con-

ference where significant portion of this work was completed. This work is supported by NSF (PHY-0969510), DOE (DE-FG02-12ER41809, DE-SC0007863), IBS (IBS-R018-D1), and the Korean Ministry of Education (NRF-2013R1A1A2061561).

-
- [1] ATLAS Collaboration [ATLAS Collaboration], ATLAS-CONF-2015-081
- [2] CMS Collaboration [CMS Collaboration], CMS-PAS-EXO-15-004.
- [3] C. Petersson and R. Torre, arXiv:1512.05333 [hep-ph]. M. Low, A. Tesi and L. T. Wang, arXiv:1512.05328 [hep-ph]. S. D. McDermott, P. Meade and H. Rami, arXiv:1512.05326 [hep-ph]. T. Higaki, K. S. Jeong, N. Kitajima and F. Takahashi, arXiv:1512.05295 [hep-ph]. E. Molinaro, F. Sannino and N. Vignaroli, arXiv:1512.05334 [hep-ph]. R. S. Gupta, S. Jäger, Y. Kats, G. Perez and E. Stamou, arXiv:1512.05332 [hep-ph]. B. Bellazzini, R. Franceschini, F. Sala and J. Serra, arXiv:1512.05330 [hep-ph]. J. Ellis, S. A. R. Ellis, J. Quevillon, V. Sanz and T. You, arXiv:1512.05327 [hep-ph]. A. Pilaftsis, arXiv:1512.04931 [hep-ph]. S. Knapen, T. Melia, M. Papucci and K. Zurek, arXiv:1512.04928 [hep-ph]. A. Angelescu, A. Djouadi and G. Moreau, arXiv:1512.04921 [hep-ph]. S. Di Chiara, L. Marzola and M. Raidal, arXiv:1512.04939 [hep-ph]. R. Franceschini *et al.*, arXiv:1512.04933 [hep-ph]. D. Buttazzo, A. Greljo and D. Marzocca, arXiv:1512.04929 [hep-ph]. Y. Nakai, R. Sato and K. Tobioka, arXiv:1512.04924 [hep-ph]. M. Backovic, A. Mariotti and D. Redigolo, arXiv:1512.04917 [hep-ph]. K. Harigaya and Y. Nomura, arXiv:1512.04850 [hep-ph]. Y. Mambrini, G. Arcadi and A. Djouadi, arXiv:1512.04913 [hep-ph]. B. Dutta, Y. Gao, T. Ghosh, I. Gogoladze and T. Li, arXiv:1512.05439 [hep-ph]. S. Matsuzaki and K. Yamawaki, arXiv:1512.05564 [hep-ph]. R. Martinez, F. Ochoa and C. F. Sierra, arXiv:1512.05617 [hep-ph]. P. Cox, A. D. Medina, T. S. Ray and A. Spray, arXiv:1512.05618 [hep-ph]. D. Becirevic, E. Bertuzzo, O. Sumensari and R. Z. Funchal, arXiv:1512.05623 [hep-ph]. J. M. No, V. Sanz and J. Setford, arXiv:1512.05700 [hep-ph]. S. V. Demidov and D. S. Gorbunov, arXiv:1512.05723 [hep-ph]. W. Chao, R. Huo and J. H. Yu, arXiv:1512.05738 [hep-ph]. S. Fichet, G. von Gersdorff and C. Royon, arXiv:1512.05751 [hep-ph]. D. Curtin and C. B. Verhaaren, arXiv:1512.05753 [hep-ph]. L. Bian, N. Chen, D. Liu and J. Shu, arXiv:1512.05759 [hep-ph]. P. Agrawal, J. Fan, B. Heidenreich, M. Reece and M. Strassler, arXiv:1512.05775 [hep-ph]. C. Csaki, J. Hubisz and J. Terning, arXiv:1512.05776 [hep-ph]. A. Falkowski, O. Slone and T. Volansky, arXiv:1512.05777 [hep-ph]. D. Aloni, K. Blum, A. Dery, A. Efrati and Y. Nir, arXiv:1512.05778 [hep-ph]. Y. Bai, J. Berger and R. Lu, arXiv:1512.05779 [hep-ph]. J. Chakraborty, A. Choudhury, P. Ghosh, S. Mondal and T. Srivastava, arXiv:1512.05767 [hep-ph]. Q. H. Cao, Y. Liu, K. P. Xie, B. Yan and D. M. Zhang, arXiv:1512.05542 [hep-ph]. J. Bernon and C. Smith, arXiv:1512.06113 [hep-ph]. A. Kobakhidze, F. Wang, L. Wu, J. M. Yang and M. Zhang, arXiv:1512.05585 [hep-ph]. A. Ahmed, B. M. Dillon, B. Grzadkowski, J. F. Guion and Y. Jiang, arXiv:1512.05771 [hep-ph]. L. M. Carpenter, R. Colburn and J. Goodman, arXiv:1512.06107 [hep-ph]. E. Megias, O. Pujolas and M. Quiros, arXiv:1512.06106 [hep-ph]. A. Alves, A. G. Dias and K. Sinha, arXiv:1512.06091 [hep-ph]. E. Gabrielli, K. Kannike, B. Mele, M. Raidal, C. Spethmann and H. Veermäe, arXiv:1512.05961 [hep-ph]. J. S. Kim, J. Reuter, K. Rolbiecek and R. R. de Austri, arXiv:1512.06083 [hep-ph]. R. Benbrik, C. H. Chen and T. Nomura, arXiv:1512.06028 [hep-ph]. S. Ghosh, A. Kundu and S. Ray, arXiv:1512.05786 [hep-ph].
- [4] T. Han, I. W. Kim and J. Song, Phys. Lett. B **693**, 575 (2010) doi:10.1016/j.physletb.2010.09.010 [arXiv:0906.5009 [hep-ph]].
- [5] K. Agashe, D. Kim, M. Toharia and D. G. E. Walker, Phys. Rev. D **82**, 015007 (2010) doi:10.1103/PhysRevD.82.015007 [arXiv:1003.0899 [hep-ph]].
- [6] W. S. Cho, D. Kim, K. T. Matchev and M. Park, Phys. Rev. Lett. **112**, no. 21, 211801 (2014) doi:10.1103/PhysRevLett.112.211801 [arXiv:1206.1546 [hep-ph]].
- [7] ROOT-‘A Data Analysis Framework’.
- [8] K. Agashe, R. Franceschini and D. Kim, Phys. Rev. D **88**, no. 5, 057701 (2013) [arXiv:1209.0772 [hep-ph]].
- [9] F. W. Stecker, “Cosmic gamma rays,” *NASA Special Publication* **249** (1971).
- [10] C. Y. Chen, H. Davoudiasl and D. Kim, Phys. Rev. D **89**, no. 9, 096007 (2014) [arXiv:1403.3399 [hep-ph]].
- [11] K. Agashe, R. Franceschini and D. Kim, JHEP **1411**, 059 (2014) [arXiv:1309.4776 [hep-ph]].
- [12] L. T. Wang and I. Yavin, JHEP **0704**, 032 (2007) doi:10.1088/1126-6708/2007/04/032 [hep-ph/0605296].
- [13] M. Burns, K. Kong, K. T. Matchev and M. Park, JHEP **0810**, 081 (2008) doi:10.1088/1126-6708/2008/10/081 [arXiv:0808.2472 [hep-ph]].
- [14] L. Edelhauser, K. T. Matchev and M. Park, JHEP **1211**, 006 (2012) doi:10.1007/JHEP11(2012)006 [arXiv:1205.2054 [hep-ph]].